2011

Analysis of Electrodeposited Nickel-Iron Alloy Film Composition Using Particle-Induced X-Ray Emission

Alyssa Frey
Hope College

Nicholas Wozniak
Hope College, nicholas.wozniak@hope.edu

Timothy Nagi
Hope College, timothy.nagi@hope.edu

Matthew Keller
Hope College, matthew.keller@hope.edu

J. Mark Lunderberg
Hope College, justin.lunderberg@hope.edu

See next page for additional authors

Published in: *International Journal of Electrochemistry*, Volume 2011, January 1, 2011, pages 604395-. The final published version is available at: http://dx.doi.org/10.4061/2011/604395

SAGE-Hindawi Access to Research
International Journal of Electrochemistry
Volume 2011, Article ID 604395, 7 pages
doi:10.4061/2011/604395

Research Article

Analysis of Electrodeposited Nickel-Iron Alloy Film Composition Using Particle-Induced X-Ray Emission

Alyssa A. Frey,[1,2] Nicholas R. Wozniak,[1] Timothy B. Nagi,[1] Matthew P. Keller,[1] J. Mark Lunderberg,[1,3] Graham F. Peaslee,[4] Paul A. DeYoung,[1] and Jennifer R. Hampton[1]

[1] *Department of Physics, Hope College, Holland, MI 49423, USA*
[2] *Department of Materials Science and Engineering, University of Wisconsin-Madison, Madison, WI 53706, USA*
[3] *Medical Scientist Training Program, The University of Chicago, Chicago, IL 60637, USA*
[4] *Department of Chemistry, Hope College, Holland, MI 49423, USA*

Correspondence should be addressed to Jennifer R. Hampton, hampton@hope.edu

Received 13 May 2011; Accepted 30 June 2011

Academic Editor: Angela Molina

The elemental composition of electrodeposited NiFe thin films was analyzed with particle-induced X-ray emission (PIXE). The thin films were electrodeposited on polycrystalline Au substrates from a 100 mM $NiSO_4$, 10 mM $FeSO_4$, 0.5 M H_3BO_3, and 1 M Na_2SO_4 solution. PIXE spectra of these films were analyzed to obtain relative amounts of Ni and Fe as a function of deposition potential and deposition time. The results show that PIXE can measure the total deposited metal in a sample over at least four orders of magnitude with similar fractional uncertainties. The technique is also sensitive enough to observe the variations in alloy composition due to sample nonuniformity or variations in deposition parameters.

1. Introduction

Electrodeposition is an attractive method for the fabrication of thin metal films and layered structures. Structures with a wide range of compositions, morphologies, and functionalities can be deposited by varying the large number of experimental parameters available in electrochemical methods. In addition, electrochemistry offers a low-cost alternative to more involved deposition techniques, such as molecular beam epitaxy or vapor deposition while producing samples with comparable purity levels [1].

When two or more metals are electrodeposited simultaneously, the elemental composition of the resulting film does not necessarily reflect the composition of the deposition solution. In particular, for binary alloys of two iron group metals (iron, cobalt, and nickel) and alloys of iron group metals with zinc or cadmium, the less noble metal deposits preferentially for a wide range of deposition conditions [2, 3]. This effect, known as "anomalous codeposition," results in a larger concentration of the less noble metal in the film than in the solution. The extent of the anomalous behavior for a particular alloy system has been shown to depend on a variety of experimental parameters including metal concentrations in solution, pH, presence of additives, deposition potential, deposition current density, and agitation of the solution during deposition [2–25].

The alloy composition of electrodeposited films has been measured by a number of different methods. A common technique is atomic absorption (AA) spectroscopy [4, 5, 7–15, 26]. In this procedure, the deposit is chemically etched from the substrate, and the ion concentrations in the resulting solution are analyzed. Because this method is destructive, the resulting sample cannot be subjected to additional analysis. A further disadvantage of AA spectroscopy is that it gives the average composition over the entire deposited sample and is not sensitive to spatial variations in stoichiometry.

Another procedure for alloy composition analysis, stripping voltammetry using a rotating ring-disk electrode (RRDE), was developed by Andricacos and coworkers [27]. This method was initially demonstrated for NiFe films and relied on the oxidation of stripped Fe^{2+} ions to Fe^{3+} at the ring of the RRDE to quantify the Fe content in the film.

Other alloy combinations can be analyzed in a similar fashion by choosing an electrochemical reaction to monitor at the ring involving only one of the species stripped from the disk [6, 28–33]. This method suffers from the same disadvantages as AA spectroscopy; it is destructive and only measures the average composition of the deposit. Additionally, the alloy deposition must be performed on the disk of an RRDE, limiting the types of substrate that can be studied.

Nondestructive analytical techniques that have been used for alloy composition determination include X-ray fluorescence (XRF) [4, 17–19, 24, 34] and energy-dispersive spectroscopy (EDS) using a scanning electron microscope (SEM) [16, 21–23, 25, 35]. In these methods, the sample is irradiated with either high-energy X-rays (XRF) or electrons (SEM-EDS) which eject electrons from atoms in the sample. These atoms then emit characteristic X-rays when the vacancies left by the ejected inner-shell electrons are filled by higher-shell electrons. The spectrum of the emitted X-rays is analyzed to determine the elemental composition of the sample. Because these methods are nondestructive, the electrodeposited films can be subjected to further analysis.

Here we describe the use of particle-induced X-ray emission (PIXE) to determine the elemental composition of electrodeposited alloy samples. As in XRF and SEM-EDS, the PIXE technique is nondestructive, particularly for inorganic materials such as metal alloys. In PIXE, a sample is irradiated with a beam of protons which eject electrons from the atoms in the sample [36]. Similar to XRF and SEM-EDS, when a higher-shell electron fills a vacancy left by an ejected inner-shell electron, an X-ray is emitted which is characteristic of the atom. A spectrum of emitted X-rays can then be analyzed to determine the elemental composition of the sample.

The primary difference between these X-ray spectroscopy techniques is the excitation mechanism: X-ray photons in XRF, electrons in SEM-EDS, and protons in PIXE. Of all three techniques, PIXE is the most sensitive to high atomic numbers because of the higher excitation energy available during the atomic collisions with protons at MeV energies. SEM-EDS typically has thinner detector windows because there are no backscattered protons, and therefore is particulary sensitive to lighter elements. XRF can measure both light and heavy elements but with less sensitivity in general depending on the X-ray source flux. By focusing the proton beam, PIXE has the capability to measure spatial variations of the film composition on the scale of a few tens of μm. One advantage that PIXE has over both SEM-EDS and XRF is that by varying the energy of the incident protons, it is also possible to control the penetration depth sampled by this technique, which can be significantly greater (up to 50–100 μm) than that obtained by XRF or SEM-EDS. This is important when considering surface fluctuations in both morphology and composition which are typically less of an issue in thick-target PIXE analyses.

PIXE has been used for trace element determination in samples such as lake sediment [37], sand dust particles [38], and gunshot residue [39]. Other recent applications include biological samples such as metal-accumulating plants [40], tree rings [41], and dental enamel [42] and archeological artifacts such as gold jewelry [43], stained glass [44], and paintings [45].

2. Experimental Details

2.1. Electrodeposition. To demonstrate the utility of PIXE for nondestructive alloy composition analysis, a set of NiFe thin films were electrodeposited on polycrystalline Au working electrodes. The working electrodes were diced from a silicon wafer plated with 1000 Å of gold over 50 Å of titanium (for adhesion; Platypus Technologies, LLC, Madison, WI). Electrodepositions were carried out using a BAS Epsilon Electrochemical Workstation (Bioanalytical Systems, Inc., West Lafayette, IN) and a custom-built Teflon cell described elsewhere [46] with a platinum wire (Alfa Aesar, Ward Hill, MA) counter electrode and an Ag/AgCl (3 M NaCl) reference electrode (Bioanalytical Systems, Inc., West Lafayette, IN). All potentials are reported with respect to this reference electrode. The films were deposited from 100 mM $NiSO_4$, 10 mM $FeSO_4$, 0.5 M H_3BO_3, and 1 M Na_2SO_4 solutions made using water that had been purified through successive reverse osmosis, deionization, and UV purification stages. All chemicals were purchased from Sigma-Aldrich (St. Louis, MO) and used as received. All depositions were carried out at room temperature.

DC potential amperometry was used to deposit the thin films. The potential of the working electrode was stepped from 0 mV to the deposition potential (which varied from −700 mV to −1200 mV) for the duration of the deposition (either 6 or 60 min), and the current was recorded as a function of time. The cathodic current for each deposition was integrated as a function of time to obtain the total deposition charge for the sample.

2.2. Particle-Induced X-Ray Emission. The elemental compositions of the deposited films were characterized with particle-induced X-ray emission (PIXE). In some cases the samples were irradiated at several locations across the sample. Specifically, proton beams with an energy of 2.3 or 3.4 MeV and beam currents in the range of 0.2–8.0 nA were produced with the 1.7 MV tandem Pelletron particle accelerator at the Hope College Ion Beam Analysis Laboratory (HIBAL). The emitted X-rays were detected with a Si(Li) detector, and a 20 mil Mylar filter was placed between the sample and the detector to reduce the detection of low-energy X-rays (Bremsstrahlung radiation and from the Si substrate).

Figure 1 shows an X-ray spectrum for a typical electrodeposited NiFe film. The X-ray energies in a PIXE spectrum reveal the elements present in the sample, while the number of X-rays detected at a particular energy is proportional to the amount of that element present. The concentrations in parts per million by weight for each element were determined with the commercial fitting program GUPIXWin. Within the program, the samples were modeled as a Si substrate with a homogeneous thin film composed of Ti, Au, Ni, and Fe. This is a reasonable model of the actual sample geometry, because the layered structure (NiFe/Au/Ti) was at most ∼3000 nm thick.

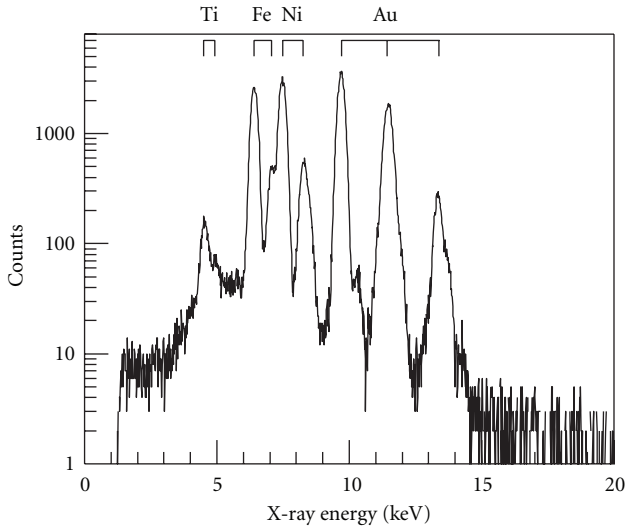

Figure 1: A PIXE spectrum of a NiFe thin film deposited from a 100 mM $NiSO_4$, 10 mM $FeSO_4$, 0.5 M H_3BO_3, and 1 M Na_2SO_4 solution at −900 mV for 6 min. Approximately 1.8 μC of 3.4 MeV protons were incident on the sample to obtain this spectrum. The peaks corresponding to the K X-rays of Ti, Fe, and Ni, and the L X-rays of Au are indicated.

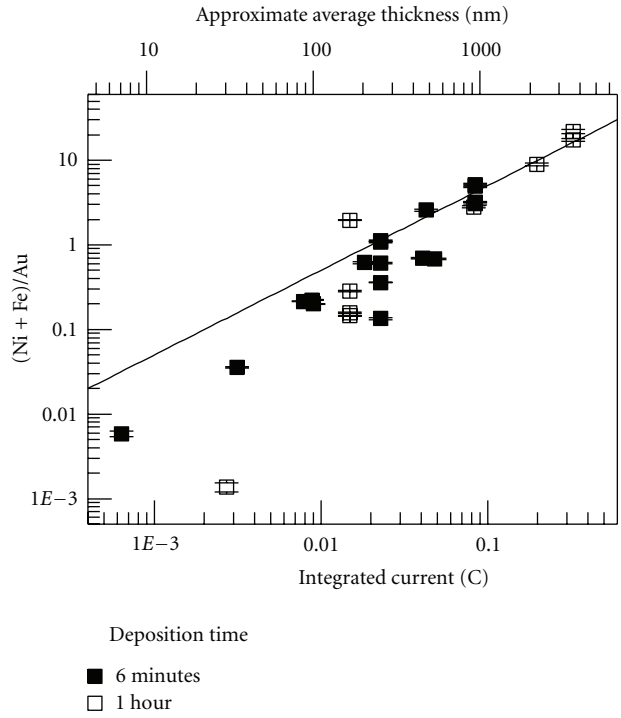

Figure 2: The (Ni + Fe)/Au ratio determined by PIXE as a function of the integrated deposition current for all the samples. The deposition potentials varied from −700 mV to −1200 mV and the deposition times were either 6 or 60 min. The upper horizontal axis indicates an approximate average deposit thickness, calculated assuming 100% current efficiency. The solid line with a slope of unity is a guide to the eye. The (Ni + Fe)/Au results fall below this line at lower integrated currents.

The Ti, Au, Ni, and Fe concentrations obtained from GUPIXWin for each PIXE spectrum were used to deduce the composition of the films. Rather than depending on absolute beam current measurements to determine the elemental concentrations, the concentrations ratios of Ni and Fe to Au for each sample were calculated. Because the working electrodes were all cut from a single, uniform Au/Ti/Si wafer, the samples had a constant amount of gold. Simulations with GUPIXWin show that for all the film thicknesses in this study, the attenuation of Au X-rays due to the NiFe film is negligible. The calculated Ni/Au and Fe/Au ratios can then be compared from sample to sample.

2.3. Scanning Electron Microscope Energy-Dispersive Spectroscopy. For comparison to the PIXE results, the compositions of the electrodeposited films were also measured with a TM3000 TableTop SEM (Hitachi, Tokyo Japan) with a Quantax 70 EDS attachment (Bruker, Madison, WI). Specifically, SEM-EDS spectra were taken over several field of view sizes (1000x–20,000x) with an accelerating voltage of 15 kV. The Quantax 70 software was used to extract Ni and Fe weight percentages from the X-ray spectra. The unweighted averages of the results from each field of view size, along with the standard deviation of the mean for the measurements, are reported.

3. Results and Discussion

3.1. Total Deposited Material to Gold Ratios. The ratio of the total amount of electrodeposited material to the amount of gold, (Ni + Fe)/Au, for each sample is shown in Figure 2 as a function of the integrated electrodeposition current for each sample. The error bars shown in the figure were calculated from the statistical and fit uncertainties obtained from the GUPIXWin analysis of the X-ray spectra. The total amount of deposited material in the samples, as determined by the (Ni + Fe)/Au ratio, varies over four orders of magnitude, and all the measurements have comparable fractional uncertainties (on the level of a few percent). This shows that the sensitivity of the PIXE measurements is sufficient to measure the total amount of deposited material over this wide range.

A deposit thickness, t, corresponding to each total charge, Q, is indicated on the upper horizontal axis in the figure. This approximate average thickness was calculated assuming 100% current efficiency from $t = Q/(neA\rho^*)$, where $n = 2$ is the number of electrons in the Ni or Fe deposition reaction, A is the area of the working electrode, and ρ^* is the number density of the deposit. The electrochemical area of the working electrode, 0.032 cm^2, was measured with cyclic voltammetry [46]. The number density for the deposit was calculated from the bulk densities of Ni and Fe and assuming a 75% Ni and 25% Fe film (in the middle of the range of measured compositions).

A linear dependence of the (Ni + Fe)/Au ratio on the integrated deposition current is evidence of a constant current efficiency. A line with a slope of unity is included in Figure 2 to show the linear relationship that exists for

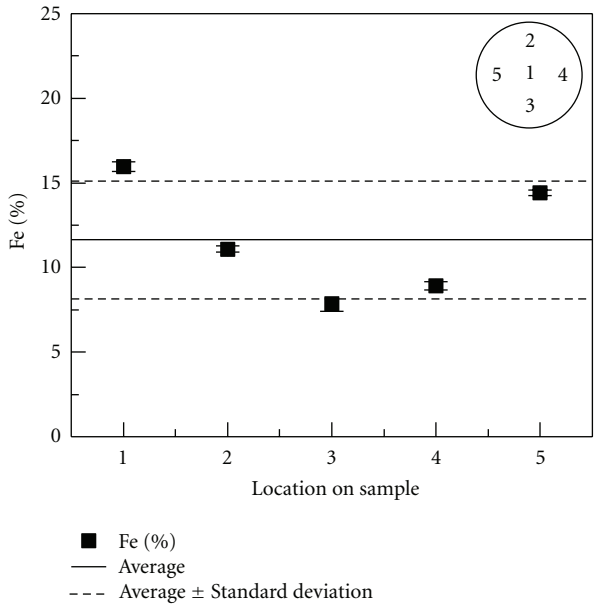

Figure 3: The iron content (percent by weight, Fe/(Ni + Fe) × 100%,) for five locations on one electrodeposited sample determined by PIXE. The NiFe thin film was deposited from a 100 mM $NiSO_4$, 10 mM $FeSO_4$, 0.5 M H_3BO_3, and 1 M Na_2SO_4 solution at −1000 mV for 6 min. A sketch of the different locations on the sample is included in the inset. The unweighted average of the results is indicated by the solid line while the dashed lines represent the average plus and minus the standard deviation.

these samples at high total deposition charges. At low total deposition charges, the (Ni + Fe)/Au ratio falls below this linear trend, indicating a lower current efficiency in that range. This result is evidence that the assumption of 100% current efficiency which was made to calculate the deposit thicknesses in the figure is not always valid. However, the result is consistent with previous studies of iron group metal deposition. The measured current efficiency for both single metal and alloy deposition generally decreases with decreasing current density (due to concurrent hydrogen evolution) and in many cases approaches 100% at higher current densities [5–8, 11, 13–15, 17, 18, 21, 24].

3.2. Sample Uniformity. To investigate the uniformity of the NiFe electrodeposited samples, the ∼1 mm diameter proton beam was moved to five different locations on a single sample (∼2 mm in diameter) and PIXE spectra were taken at each location. The iron content as a percent of the total deposited material, Fe/(Ni + Fe) × 100%, for each location is shown in Figure 3. As in Figure 2, the error bars were calculated from the statistical and fit uncertainties from the GUPIXWin analysis. The unweighted average and the standard deviation of the five measurements are also indicated in the figure by the solid and dashed lines, respectively. For this sample, the variation in iron content between measurements is larger than the uncertainties for each individual measurement. PIXE analysis is sensitive enough to observe these variations across a single sample and from sample to sample.

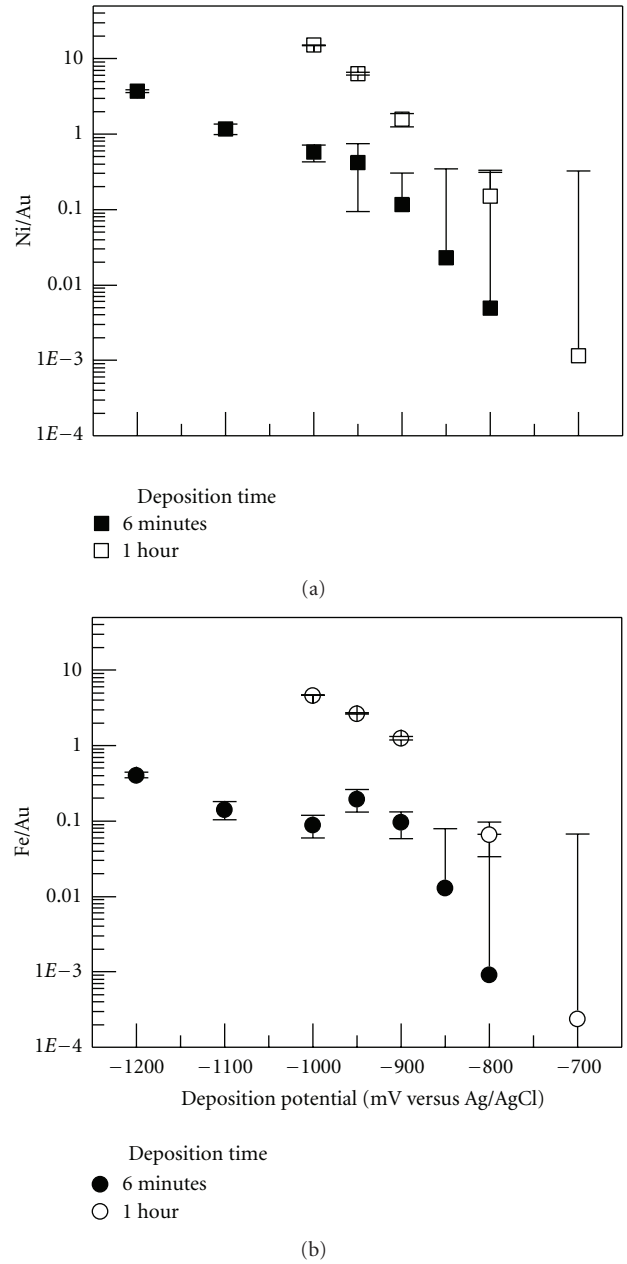

Figure 4: The (a) Ni/Au ratio and (b) Fe/Au ratio determined by PIXE as a function of the deposition potential for two different deposition times.

3.3. Single Metal to Gold Ratios. In order to investigate the deposition rate of iron and nickel separately, the individual metal-to-gold ratios, Ni/Au and Fe/Au, are graphed in Figure 4 as a function of deposition potential. To observe the trends in sample composition due to the deposition parameters, the average results over several replicate measurements are shown. The error bars in the figure are the standard deviation of the results in Figure 3 (the sample with the most replicates measured) divided by the square root of the number of replicates measured for that particular sample.

At less negative potentials, both the Ni and Fe deposition rates show an exponential dependence on the potential,

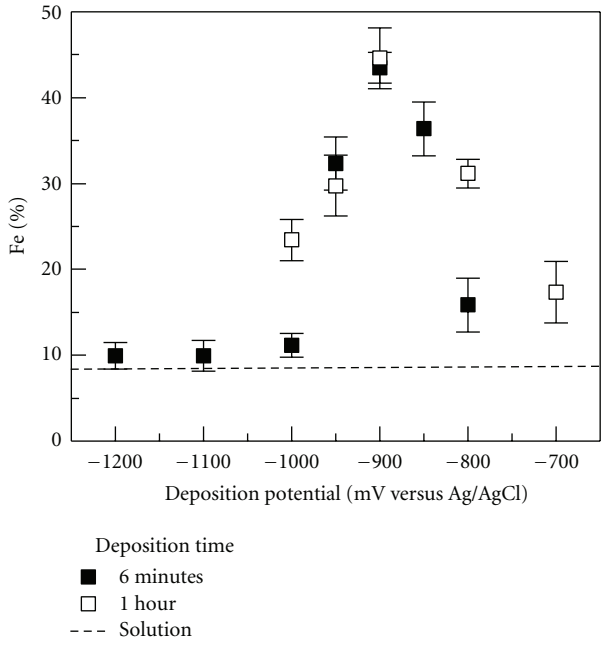

Figure 5: The iron content (percent by weight, Fe/(Ni + Fe) × 100%) in the electrodeposited films determined by PIXE as a function of deposition potential for two different deposition times. The Fe content in the deposition solution (8.7%) is indicated by the dashed line.

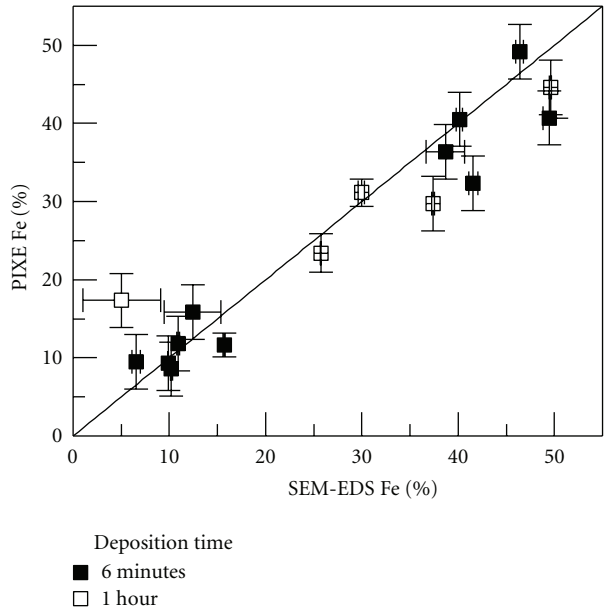

Figure 6: The iron content (percent by weight, Fe/(Ni + Fe) × 100%) in the electrodeposited films determined by PIXE as a function of the iron content (percent by weight) determined by SEM-EDS. The solid line with a slope of unity and an intercept of zero is a guide to the eye.

as predicted by the Butler-Volmer equation for kinetically limited reactions [47]. At more negative potentials, the exponential dependence is no longer evident, suggesting the beginning of mass-transport limited reaction rates. As expected, for a given potential, the films that were deposited for a longer amount of time contained more of each metal than did the films deposited for a shorter amount of time. These results demonstrate the reliability of using PIXE as a method of analysis.

3.4. Percent of Deposit. Figure 5 shows the Fe content in the deposited films as a percent of the total deposited material, Fe/(Ni + Fe) × 100%, as a function of deposition potential. Again, average results from several replicate measurements are shown. Two results are clear. First, these films exhibit anomalous codeposition. For a wide range of potentials, the Fe content in the films is larger than the corresponding Fe content in the solution (indicated with the dashed line). Second, the amount of this anomalous codeposition changes with the deposition potential and (to a lesser extent) the deposition time. A peak in the Fe content is seen at approximately −900 mV for this set of deposition conditions. This peak was obtained for both the 6-minute films and the 1-hour films. Similar behavior has been seen by a number of groups for a variety of iron group alloy combinations and deposition conditions [5–7, 9, 10, 14].

3.5. Comparison to Scanning Electron Microscope Energy-Dispersive Spectroscopy Measurements. Figure 6 shows the Fe content in the deposited films as determined by PIXE compared to that determined by the more traditional SEM-EDS analysis. A line indicating the ideal case of elemental iron concentration measured by PIXE being exactly equal to the concentration measured by SEM-EDS is included in the figure for comparison. Over the entire range of compositions measured in this study, the PIXE results compare favorably to the SEM-EDS results, which lends support that the PIXE measurements are reliable for determining the composition of these electrodeposited thin films.

4. Conclusion

The results presented here show that particle-induced X-ray emission is a useful analytical tool to examine the composition of electrodeposited alloy thin films. For the Au/Ti/Si substrates used here, by calculating the ratio of the amount of nickel and iron observed to the amount of gold (which is a constant), the relative amounts of the deposited metals can be compared between samples. Using the same procedure, samples with four orders of magnitude difference in total deposited material were measured with comparable fractional uncertainties (at the level of a few percent). PIXE also has the sensitivity to measure variations in elemental content due to sample non uniformity or to changes in deposition conditions.

Acknowledgments

The authors thank Dave Daugherty for his dedication to accelerator operations. This paper is based upon work supported by the National Science Foundation under Grants

no. REU-PHY-0452206, MRI-0319523, and MRI-0959282, the Hope College Dean for the Natural and Applied Sciences Office, and the Hope College Department of Physics.

References

[1] W. Schindler and J. Kirschner, "Ultrathin magnetic films: electrochemistry versus molecular-beam epitaxy," *Physical Review B*, vol. 55, no. 4, pp. R1989–R1992, 1997.

[2] A. Brenner, *Electrodeposition of Alloys: Principles and Practice*, vol. 1, Academic Press, New York, NY, USA, 1963.

[3] T. Akiyama and H. Fukushima, "Recent study on the mechanism of the electrodeposition of iron-group metal alloys," *ISIJ International*, vol. 32, no. 7, pp. 787–798, 1992.

[4] H. Dahms and I. M. Croll, "The anomalous codeposition of iron-nickel alloys," *Journal of The Electrochemical Society*, vol. 112, pp. 771–775, 1965.

[5] J. Horkans, "Effect of plating parameters on electrodeposited NiFe," *Journal of the Electrochemical Society*, vol. 128, no. 1, pp. 45–49, 1981.

[6] P. C. Andricacos, C. Arana, J. Tabib, J. Dukovic, and L. T. Romankiw, "Electrodeposition of nickel-iron alloys. I. Effect of agitation," *Journal of the Electrochemical Society*, vol. 136, no. 5, pp. 1336–1340, 1989.

[7] D. L. Grimmett, M. Schwartz, and K. Nobe, "Pulsed electrodeposition of iron-nickel alloys," *Journal of the Electrochemical Society*, vol. 137, no. 11, pp. 3414–3418, 1990.

[8] D. Gangasing and J. B. Talbot, "Anomalous electrodeposition of nickel-iron," *Journal of the Electrochemical Society*, vol. 138, no. 12, pp. 3605–3611, 1991.

[9] W. C. Grande and J. B. Talbot, "Electrodeposition of thin-films of nickel-iron I. Experimental," *Journal of the Electrochemical Society*, vol. 140, pp. 669–674, 1993.

[10] D. L. Grimmett, M. Schwartz, and K. Nobe, "Comparison of DC and pulsed Fe-Ni alloy deposits," *Journal of the Electrochemical Society*, vol. 140, no. 4, pp. 973–978, 1993.

[11] K. Y. Sasaki and J. B. Talbot, "Electrodeposition of binary iron-group alloys," *Journal of the Electrochemical Society*, vol. 142, no. 3, pp. 775–782, 1995.

[12] K. M. Yin and B. T. Lin, "Effects of boric acid on the electrodeposition of iron, nickel and iron-nickel," *Surface and Coatings Technology*, vol. 78, no. 1–3, pp. 205–210, 1996.

[13] T. M. Harris and J. S. Clair, "Testing the role of metal hydrolysis in the anomalous electrodeposition of Ni-Fe alloys," *Journal of the Electrochemical Society*, vol. 143, no. 12, pp. 3918–3922, 1996.

[14] K. Y. Sasaki and J. B. Talbot, "Electrodeposition of iron-group metals and binary alloys from sulfate baths: I. Experimental study," *Journal of the Electrochemical Society*, vol. 145, no. 3, pp. 981–990, 1998.

[15] S. Gadad and T. M. Harris, "Oxygen incorporation during the electrodeposition of Ni, Fe, and Ni-Fe alloys," *Journal of the Electrochemical Society*, vol. 145, no. 11, pp. 3699–3703, 1998.

[16] E. Gómez and E. Vallés, "Electrodeposition of Co+Ni alloys on modified silicon substrates," *Journal of Applied Electrochemistry*, vol. 29, no. 7, pp. 805–812, 1999.

[17] D. Golodnitsky, N. V. Gudin, and G. A. Volyanuk, "Study of nickel-cobalt alloy electrodeposition from a sulfamate electrolyte with different anion additives," *Journal of the Electrochemical Society*, vol. 147, no. 11, pp. 4156–4163, 2000.

[18] T. Nakanishi, M. Ozaki, H. S. Nam, T. Yokoshima, and T. Osaka, "Pulsed electrodeposition of nanocrystalline CoNiFe soft magnetic thin films," *Journal of the Electrochemical Society*, vol. 148, no. 9, pp. C627–C631, 2001.

[19] Y. Zhuang and E. J. Podlaha, "NiCoFe ternary alloy deposition II. Influence of electrolyte concentration at steady state," *Journal of the Electrochemical Society*, vol. 150, no. 4, pp. C219–C224, 2003.

[20] R. Oriňáková, A. Turoňová, D. Kladeková, M. Gálová, and R. M. Smith, "Recent developments in the electrodeposition of nickel and some nickel-based alloys," *Journal of Applied Electrochemistry*, vol. 36, no. 9, pp. 957–972, 2006.

[21] D. Y. Park, K. S. Park, J. M. Ko et al., "Electrodeposited $Ni_{1-x}Co_x$ nanocrystalline thin films," *Journal of the Electrochemical Society*, vol. 153, no. 12, Article ID 021612JES, pp. C814–C821, 2006.

[22] E. Beltowska-Lehman and P. Indyka, "Electrodeposition and characterisation of thin magnetic Ni-Fe films on copper substrates," *Archives of Metallurgy and Materials*, vol. 53, no. 1, pp. 97–101, 2008.

[23] C. K. Chung and W. T. Chang, "Effect of pulse frequency and current density on anomalous composition and nanomechanical property of electrodeposited Ni-Co films," *Thin Solid Films*, vol. 517, no. 17, pp. 4800–4804, 2009.

[24] S. Riemer, J. Gong, M. Sun, and I. Tabakovic, "Influence of solution pH and concentration of saccharin on electrodeposition and properties of 2.4 T CoFe alloys," *Journal of the Electrochemical Society*, vol. 156, no. 10, pp. D439–D447, 2009.

[25] L. D. Rafailović, H. P. Karnthaler, T. Trišović, and D. M. Minić, "Microstructure and mechanical properties of disperse Ni-Co alloys electrodeposited on Cu substrates," *Materials Chemistry and Physics*, vol. 120, no. 2-3, pp. 409–416, 2010.

[26] M. Ghorbani, A. G. Dolati, and A. Afshar, "Electrodeposition of Ni-Fe alloys in the presence of complexing agents," *Russian Journal of Electrochemistry*, vol. 38, no. 11, pp. 1173–1177, 2002.

[27] P. C. Andricacos, J. Tabib, and L. T. Romankiw, "Stripping voltammetry of nickel-iron films electrodeposited on platinum using a rotating-ring-disk electrode," *Journal of the Electrochemical Society*, vol. 135, pp. 1172–1174, 1988.

[28] K. H. Wong and P. C. Andricacos, "Composition determination of electrodeposited NiSn and PbSn alloys using stripping voltammetry at a rotating ring-disk electrode," *Journal of the Electrochemical Society*, vol. 137, no. 4, pp. 1087–1090, 1990.

[29] J. Horkans, I. C. Hsu Chang, P. C. Andricacos, and E. J. Podlaha, "Determination of partial currents for CuNi and CuCo electrodeposition using rotating ring-disk electrodes," *Journal of the Electrochemical Society*, vol. 138, no. 2, pp. 411–416, 1991.

[30] P. C. Andricacos, "Composition determination of NiCo alloys by the RRDE method," *Journal of the Electrochemical Society*, vol. 142, no. 6, pp. 1824–1828, 1995.

[31] J. A. Mitchell, W. R. Pitner, C. L. Hussey, and G. R. Stafford, "Electrodeposition of cobalt and cobalt-aluminum alloys from a room temperature chloroaluminate molten salt," *Journal of the Electrochemical Society*, vol. 143, no. 11, pp. 3448–3455, 1996.

[32] S. D. Leith and D. T. Schwartz, "Flow-induced composition modulated NiFe thin films with nanometer-scale wavelengths," *Journal of the Electrochemical Society*, vol. 143, no. 3, pp. 873–878, 1996.

[33] S. D. Leith, S. Ramli, and D. T. Schwartz, "Characterization of Ni_xFe_{1-x} $(0.10 < x < 0.95)$ electrodeposition from a family of sulfamate-chloride electrolytes," *Journal of the Electrochemical Society*, vol. 146, no. 4, pp. 1431–1435, 1999.

[34] N. Zech, E. J. Podlaha, and D. Landolt, "Anomalous codeposition of iron group metals I. Experimental results," *Journal of the Electrochemical Society*, vol. 146, no. 8, pp. 2886–2891, 1999.

[35] E. M. Kakuno, D. H. Mosca, I. Mazzaro et al., "Structure, composition, and morphology of electrodeposited Co_xFe_{1-x} alloys," *Journal of the Electrochemical Society*, vol. 144, no. 9, pp. 3222–3226, 1997.

[36] S. A. E. Johansson, J. L. Campbell, and K. G. Malmqvist, *Particle-Induced X-Ray Emission Spectrometry (PIXE)*, Wiley, New York, NY, USA, 1995.

[37] J. M. Lunderberg, R. J. Bartlett, A. M. Behm et al., "PIXE as a complement to trace metal analysis of sediments by ICP-OES," *Nuclear Instruments and Methods in Physics Research B*, vol. 266, no. 21, pp. 4782–4787, 2008.

[38] S. Matsuyama, K. Ishii, H. Yamazaki et al., "Microbeam analysis of yellow sand dust particles," *X-Ray Spectrometry*, vol. 37, no. 2, pp. 151–155, 2008.

[39] M. J. Bailey, K. J. Kirkby, and C. Jeynes, "Trace element profiling of gunshot residues by PIXE and SEM-EDS: a feasibility study," *X-Ray Spectrometry*, vol. 38, no. 3, pp. 190–194, 2009.

[40] R. Siegele, A. G. Kachenko, N. P. Bhatia et al., "Localisation of trace metals in metal-accumulating plants using μ-PIXE," *X-Ray Spectrometry*, vol. 37, no. 2, pp. 133–136, 2008.

[41] A. R. Cruz-Muñoz, L. Rodríguez-Fernández, G. Calva-Vázquez, and J. L. Ruvalcaba-Sil, "Effects due to Popocatepetl volcano eruptions on the elemental concentrations in tree growth rings," *X-Ray Spectrometry*, vol. 37, no. 2, pp. 163–168, 2008.

[42] E. A. Preoteasa, E. Preoteasa, A. Kuczumow et al., "Broad-beam PIXE and μ-PIXE analysis of normal and in vitro demineralized dental enamel," *X-Ray Spectrometry*, vol. 37, no. 5, pp. 517–535, 2008.

[43] B. Constantinescu, R. Bugoi, V. Cojocaru et al., "Micro-SR-XRF and micro-PIXE studies for archaeological gold identification—the case of Carpathian (Transylvanian) gold and of Dacian bracelets," *Nuclear Instruments and Methods in Physics Research B*, vol. 266, no. 10, pp. 2325–2328, 2008.

[44] T. Calligaro, "PIXE in the study of archaeological and historical glass," *X-Ray Spectrometry*, vol. 37, no. 2, pp. 169–177, 2008.

[45] L. De Viguerie, L. Beck, J. Salomon, L. Pichon, and P. Walter, "Composition of renaissance paint layers: simultaneous particle induced X-ray emission and backscattering spectrometry," *Analytical Chemistry*, vol. 81, no. 19, pp. 7960–7966, 2009.

[46] N. R. Wozniak, A. A. Frey, L. W. Osterbur, T. S. Boman, and J. R. Hampton, "An electrochemical cell for the efficient turn around of wafer working electrodes," *Review of Scientific Instruments*, vol. 81, no. 3, Article ID 034102, 2010.

[47] A. J. Bard and L. R. Faulkner, *Electrochemical Methods: Fundamentals and Applications*, Wiley, New York, NY, USA, 2nd edition, 2001.